Tailoring plasmonic resonances in Cu-Ag metal islands films

Matej Bubaš[a], Vesna Janicki[a], Stefano A. Mezzasalma[a,b], Maria Chiara Spadaro[c], Jordi Arbiol[c,d], Jordi Sancho-Parramon[a,*]

[a] *Ruđer Bošković Institute, Bijenička cesta 54, 10000 Zagreb, Croatia*
[b] *Lund Institute of Advanced Neutron and X-ray Science (LINXS), Lund University, Scheelevägen 19, 22370 Lund, Sweden*
[c] *Catalan Institute of Nanoscience and Nanotechnology (ICN2), CSIC and BIST, Campus UAB, Bellaterra, 08193 Barcelona, Catalonia, Spain*
[d] *ICREA, Pg. Lluís Companys 23, 08010 Barcelona, Catalonia, Spain*

Abstract

The plasmonic response of Cu-Ag metal islands films is investigated. Films are obtained by subsequent electron beam deposition of Ag and Cu using different fabrication conditions: deposited mass thickness, substrate temperature and post-deposition annealing in vacuum. Optical properties of films are investigated by spectroscopic ellipsometry and correlated with the structural characterization results obtained by electron microscopy. It is observed that Ag enhances island growth and increases the percolation threshold of Cu films. The localized surface plasmon resonance of isolated particles shows signatures of both Cu and Ag. Moderate thermal annealing enhances island growth and favours Janus-like morphology, increasing the Ag contribution to the surface plasmon resonance. In case of percolated films, annealing-induced dewetting can lead to the appearance of large and irregular particles with a remarkable absorption peak in the infrared range. Composition and optical

*Corresponding author. E-mail: jsancho@irb.hr

properties of the films can be further modified by Ag partial evaporation upon annealing at high temperatures. The variation of optical properties with aging is related to Cu oxidization and follows different trends depending on the sample morphology. Overall, it is shown that Cu-Ag island films are compelling systems for plasmonic applications, as their optical response can be widely and easily tuned by adjusting fabrication conditions.
Keywords:
surface plasmon resonance, metal islands films, ellipsometry, optical properties, dewetting, electron microscopy, Janus nanoparticles

1. Introduction

The large application potential of plasmonics has motivated a quest for alternative materials that can provide better performance and wavelength tuning than silver and gold. Other pure metals, nitrides, oxides, silicides and 2D materials have been proposed as potential replacement for classical plasmonics materials [1, 2]. Although many of these materials have low ohmic losses and cover a broad spectral range of plasmon resonances, they also present a very low plasma frequency that ultimately limits their performance in many standard plasmonic applications [3, 4]. Therefore, the combination of metals as alloys or hybrid nanostructures appears as one of the most prospective directions for tailoring plasmonic resonances [5, 6, 7].

In addition to the search for alternative materials, cost efficient and high throughput nano-structuring fabrication methods are key for practical implementation of plasmonic applications. In this context, well-established thin film physical vapor deposition techniques have a central role. The initial

stages of metal condensation on dielectric surfaces follow the Volmer–Weber growth mechanism that results into nearly 2-dimensional ensembles of metal nanoparticles [8, 9], known as metal islands films. Multiple metal combinations suitable for plasmonics have been used to produce alloy or hybrid island films [6, 10, 11, 12, 13, 14]. Among them, Cu-Ag systems are of special interest due to the immiscibility of these metals enabling the formation of hybrid islands. In this case, the resulting localized surface plasmon resonance (LSPR) shows signatures of both Cu and Ag individual resonances [15]. These properties have been investigated in the context of surface enhanced Raman scattering in systems obtained by simultaneous deposition of Ag and Cu via co-evaporation [16], co-sputtering [17], pulsed laser deposition [18] or dewetting after deposition [19, 20, 21]. In these studies individual islands show well-separated Cu and Ag regions forming heterodimer or Janus particles. On the other hand, subsequent deposition of Cu and Ag can result in core-shell particles [14] that transform into Janus-like particles upon annealing [22]. Although the dynamics of these morphological changes appears to be well understood [23, 24, 25] their effect on the optical response has received little attention.

In this work we investigate the plasmonic properties of Cu-Ag metal islands films fabricated by sequential deposition of Ag and Cu on glass and silicon substrates. Samples are fabricated using a wide range of conditions (deposited metal thickness, substrate temperature, post-deposition annealing) that produce different island morphology and optical properties. It is observed that Ag reduces the percolation threshold and enhances the Cu island growth. LSPR line-shape depends on film composition and islands

morphology, which can be modified upon annealing. Films deposited on substrates without pre-heating show percolated structures that can dewet into large particles with strong infrared absorption. High temperature annealing induces partial Ag evaporation, modifying the LSPR line-shape. Optical properties of samples change with aging due to Cu oxidization but follow different trends depending on the film structure. These results demonstrate that it is possible to broadly tune the optical properties of Cu-Ag islands by controlling the islands morphology through the fabrication process.

2. Materials and methods

Metal islands films were deposited on silicon and BK7 glass substrates by subsequent electron beam evaporation of Ag and Cu in a modified Varian Chamber with a base pressure of 6×10^{-7} Torr. Quartz crystal monitoring was used to control the deposited mass thickness of Ag (d_{Ag}) and Cu (d_{Cu}). Combinations with $d_{Ag} = 0$, 2, 5, 8 nm and $d_{Cu} = 5$, 10 nm were fabricated. Deposition rate for both metals was ≈ 1 Å/s. All substrates were pre-coated with a 80 nm thick SiO_2 in order to insure the same conditions for island growth regardless the substrate. Before deposition, substrates were either not pre-heated ($T_s = \mathrm{RT}$) or pre-heated at $T_s = 200$ °C. In order to enhance island growth, Ag was deposited before Cu, as Ag has worse wetting properties due to its lower surface energy on dielectric substrates [26]. In recent works it has been shown that the opposite deposition order can be used to quench Ag island growth [27]. After deposition, samples were annealed in vacuum at 450 °C and 750 °C for 1 hour to induce particle growth and dewetting of compact films [28].

Optical properties of samples were investigated by spectroscopic ellipsometry using a J. A. Woollam V-VASE ellipsometer. Measurements were done on samples deposited on Si substrates in the spectral range 0.57 - 4.5 eV and at angles of incidence of 65° and 75° . Fitting of ellipsometric data led to retrieval of the Cu-Ag film effective thickness (d_{eff}) and dielectric function (ε_{eff}). Spectral dependence of ε_{eff} was modelled using a multiple-oscillator dispersion equation with Gaussian oscillators to account for LSPR and interband transitions and a Drude term to represent connection among islands into a percolated network. This model is able to provide an accurate description of optical properties for different metal island films systems [29, 30, 31]. Transmittance measurements at normal incidence were done in the spectral range 300 - 1100 nm using a Lambda 25 Perkin-Elmer spectrophotometer. These measurements were taken at different time intervals to monitor optical response change upon sample exposition to air.

The insights obtained from optical measurements were supported by electron microscopy structural and morphological characterizations on selected samples. Scanning electron microscopy (SEM) plain view images were taken with a field-emission microscope Jeol JSM 7000F at a typical acceleration voltage of 15 kV. Scanning transmission electron microscopy (STEM) investigation was performed on a field emission gun FEI Tecnai F20 microscope. High angle annular dark-field (HAADF) STEM was combined with electron energy loss spectroscopy (EELS) in the Tecnai microscope by using a GATAN QUANTUM filter in order to obtain compositional maps. TEM samples were prepared by both, (1) via preparing cross-sectional views of the as deposited material on Si substrates, by conventional mechanical polishing

and ion milling routes and (2) by scratching the surface of the as grown sample and depositing the obtained powders on top of a carbon coated Cu grid for plain view analyses. EELS mapping was performed using the M-edge at 367 eV for Ag and the Cu L-edge at 931 eV for Cu. The O K-edge at 532 eV was used to distinguish the SiO_2 film.

Simulation of the optical response including the extinction efficiency of single particles was carried out using the MNPBEM boundary element method toolbox [32] with the aim to investigate absorption properties of core-shell and Janus nanoparticles. Optical constants of Ag and Cu used in the simulations were taken from the literature [33].

3. Results and discussion

3.1. Influence of d_{Ag} on metal islands deposited on pre-heated substrates

We start by investigating the effect of d_{Ag} on the optical and structural properties of samples with $d_{Cu} = 5$ nm that are deposited on substrates pre-heated at $T_s = 200$ °C. The imaginary part of ε_{eff} for these films is shown in the top panel of Figure 1. All samples show a major peak in the range between 1.5 and 2 eV that can be assigned to LSPR of isolated particles. This LSPR peak progressively blue-shifts and increases in strength when d_{Ag} grows. The peak has a shoulder around 2.5 eV that can be related to the presence of Ag, for it becomes more prominent at larger d_{Ag}. In fact, LSPR of small particles takes place for Ag at higher photon energies than for Cu [34]. Presence of Ag is also evident in a progressive strengthening of the peak at 4.2 eV, as it reflects the occurrence of interband transitions at the L point of Ag electronic band structure [35]. On the other hand, the film without

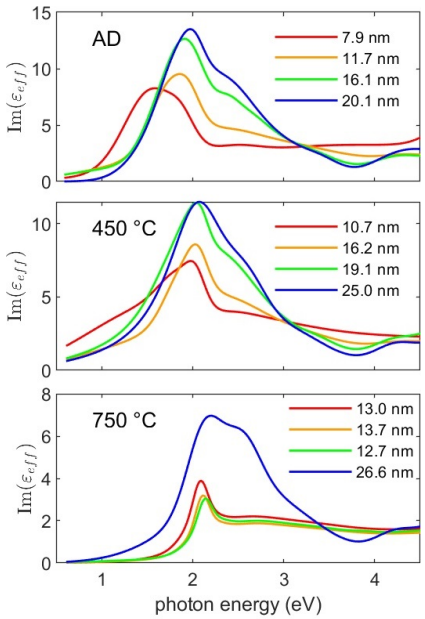

Figure 1: Imaginary part of ε_{eff} for samples deposited on pre-heated substrates with d_{Cu} = 5 nm and different d_{Ag} as a function of photon energy. Color lines indicate different Ag seeds: d_{Ag} = 0 (red), 2 (orange), 5 (green) and 8 nm (blue). Legend numbers indicate d_{eff} values for each sample. Top panel: as-deposited (AD) samples, middle panel: samples annealed at 450 °C, bottom panel: samples annealed at 750 °C.

Ag shows a nearly constant imaginary part of ε_{eff} that is correlated with the broad distribution of electronic interband absorption in Cu above 2.5 eV [33, 35]. Values of d_{eff}, shown in the Figure legend, suggest an increase of particle size in the direction perpendicular to the substrate when more Ag is deposited.

The isolated-particle morphology of these films is confirmed by scanning electron micrographs of the sample surface (Figure 2). In all cases the shape of nanoparticles is slightly elongated and irregular, and their size distribution resembles a log-normal distribution, which points to a high surface mobility

and coalescence of nanoislands during deposition [36]. Average particle size in the direction parallel to the surface (D) increases with the amount of Ag: 13.5, 14.2, 21.2 and 33.6 nm for d_{Ag} = 0, 2, 5 and 8 nm, respectively. It can be expected that particle dimensions increase with the total amount of deposited material ($d_{Ag} + d_{Cu}$). Yet, it should be noted that Volmer-Weber growth mechanism is enhanced by Ag: adding a small amount of Ag seeds (d_{Ag} = 2 nm) results in a change of the average particle aspect ratio (estimated as d_{eff}/D) from 0.59 to 0.83. A sphericity increase can contribute in fact to the large initial LSPR blue shift [37]. A further increase in Ag amount reduces the particles aspect ratio to 0.76 (d_{Ag} = 5 nm) and 0.60 (d_{Ag} = 8 nm). In addition, the overall particle density decreases from 1700 (d_{Ag} = 0 nm) to 470 (d_{Ag} = 8 nm) particles/μm^2. Observe that, as the aspect ratio is quite similar in these two samples, it cannot afford an explanation for the LSPR blue- shift in the Ag-rich films. A more promising correlation seems to be rather dictated by the large Ag content and a weaker electromagnetic coupling, as it establishes as a consequence of a larger interparticle distance [31, 29].

3.2. Annealing effects on samples deposited on pre-heated substrates

Annealing of these samples at 450 °C induces a blue shift of LSPR along with an increase of d_{eff} (middle panel in Figure 1). The shift is most evident in the sample without Ag seeds, that as-deposited shows the smallest and most closely located islands. In films containing Ag the relative weight of LSPR high-energy shoulder appears to increase. Annealing at higher temperature (750 °C, bottom panel in Figure 1) leads to more remarkable changes. Samples with d_{Ag}= 0, 2 and 5 nm have very similar optical properties, show-

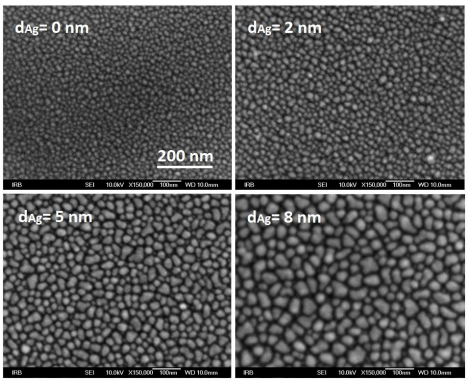

Figure 2: Scanning electron microscopy of samples with d_{Cu} = 5 nm and different d_{Ag} deposited on pre-heated substrates. All micrographs are taken at the same magnification.

ing a LSPR peak without noticeable Ag contribution. Ag interband transition peak at 4.2 eV is also absent from these samples. This behaviour can be explained by the evaporation of Ag from the film, given that Ag has nearly 3 orders of magnitude higher vapor pressure than Cu at the annealing temperature [38]. In addition, values of d_{eff} for films with d_{Ag} = 2 and 5 nm are smaller than after annealing at 450 °C, suggesting a reduced particle size due to Ag evaporation. It has been proposed that differences in evaporation rates of metals can be used as a way to control the composition and hence physical properties of hybrid nanostructures [39]. Interestingly, Ag evaporation is not evident in the film with d_{Ag} = 8 nm because the sample annealed at 750 °C shows stronger Ag contribution to LSPR and larger d_{eff} than the one annealed at 450 °C.

Scanning electron micrographs of the sample with d_{Ag} = 8 nm and d_{Cu} = 5 nm annealed at 450 °C (left panel in in Figure 3) reveal a structure similar to the as-deposited sample (D = 31.3 nm and ca. 470 particles/μm^2). The sample annealed at 750 °C (right panel in Figure 3) shows larger and

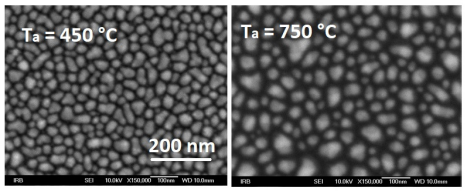

Figure 3: Scanning electron microscopy of sample with $d_{Cu} = 5$ nm and $d_{Ag} = 8$ nm deposited on pre-heated substrates and annealed at 450 (left) and 750 °C (right). All micrographs are taken at the same magnification.

more isolated particles ($D = 44$ nm and 270 particles/μm^2). Besides size and interparticle distance increase with annealing, the nanoislands size distribution still resembles log-normal distribution and their shape remains elongated. This suggests that island growth during annealing follows a similar mechanism based on island coalescence and high surface mobility as during deposition. Energy dispersion X-ray spectroscopy of surfaces investigated by SEM indicate that Cu to Ag ratio of weight concentrations is 0.41 for the sample annealed at 450 °C and 0.47 for the one annealed at 750 °C. The corresponding ratio for weight concentrations for the as deposited amount of Ag and Cu is 0.42. Thus, a mild Ag evaporation seems to takes place upon annealing at 750 °C. Nonetheless, the remaining amount of Ag influences the film optical properties more strongly than in as-deposited and moderately annealed samples.

Island brightness in the micrographs of Figure 3 suggests that islands have an inhomogeneous electron density, many of them showing a distinctive two-region structure. This inhomogeneity is more evident in the sample annealed at 750 °C. In order to get a better insight on the individual island characteristics, STEM-EELS maps of metal island film cross section were obtained

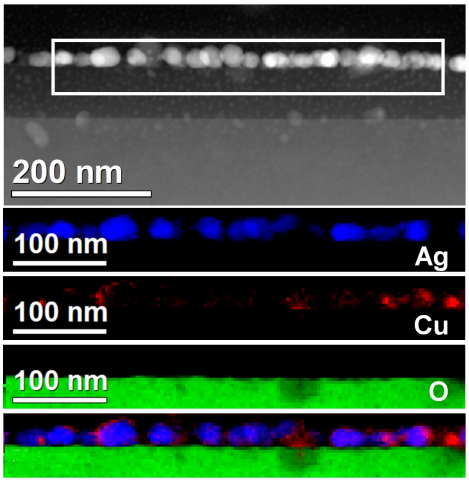

Figure 4: STEM-EELS map of the sample with $d_{Ag} = 8$ nm and $d_{Cu} = 5$ nm deposited on pre-heated substrate and annealed at 450 °C. Top panel shows islands cross section morphology while lower panels the Ag, Cu and O distribution and the combined elemental distribution.

for the sample annealed at 450 °C (Figure 4). Islands show preferentially Janus-like structures with well-separated Cu and Ag regions. Some pure Ag particles are also observed. Thus, although Cu was initially deposited on Ag, core-shell morphology is not dominant upon annealing [22]. It turns out that annealing primarily results in a redistribution of Ag and Cu atoms within islands, justifying the moderate changes in average particle size and particle density observed by SEM.

For elucidating whether the islands morphological changes can explain LSPR trends upon annealing, numerical simulations of the optical response of composite ellipsoids were carried out (Figure 5). Two geometries were considered: Ag core-Cu shell structure and Ag-Cu Janus particle, assuming in both cases a 1:1 volume contribution of Ag and Cu. The core-shell ge-

ometry is used as an approximation to represent particles where Cu coats Ag seeds. In order to make simulations consistent with experimental observations, the ellipsoid semi-axes were set to $a = 35$ nm and $b = c = 15$ nm and the refractive index of the particle environment to 1.25, i.e. a mean of the refractive index of air and SiO_2 underlayer. Light polarization parallel and perpendicular to the long semi-axes are considered because, for randomly oriented particles laying on a substrate along their major semi-axis, the normal-incidence optical response should average these polarizations. In the core-shell case ellipsoids representing the Ag core and Cu shell are concentric and have the same aspect ratio. Janus ellipsoid is split in Cu and Ag regions through the symmetry plane perpendicular to the major semi-axes. The optical response core-shell ellipsoid is dominated by a main resonance around 2 eV that can be associated with a longitudinal dipole plasmon mode, as evidenced by the calculated surface charge distribution shown in panel A. The transverse response is much weaker. For the Janus nanoparticle, spectra show three dipole-like resonances of comparable strength: a longitudinal resonance around 2 eV related to the Cu region (panel B), a longitudinal response around 2.8 eV related to the Ag region (panel C) and a transverse resonance located around 3.5 eV, also connected with the Ag region (panel D). Transverse resonance associated to Cu region is absent due to the interband transitions in the corresponding spectral region [34]. A richer spectral response of Janus ellipsoid is explained by the presence of two different materials at the particle surface. In this way, the Janus configuration enhances the role of Ag in the overall plasmonic response of nanoparticles in comparison with the Ag core - Cu shell structure. The progressive strengthening of the

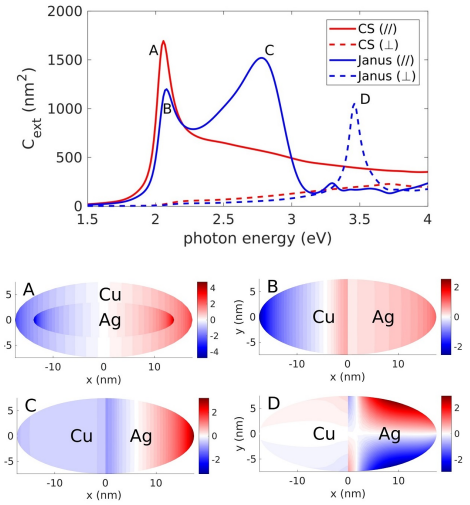

Figure 5: Top panel: computed extinction cross section of core-shell (CS) and Janus ellipsoids for light polarization parallel (∥) and perpendicular (⊥) to the major semi-axis as a function of photon energy. Lower panels show the surface charge distribution on the particle surface (at z=0) of the ellipsoid at the plasmon resonance peaks identified in the top panel.

Ag-related shoulder in the LSPR upon annealing therefore can be correlated with island morphological transitions that strengthen materials segregation [40, 22] and favour Janus-like structures.

3.3. Influence of d_{Ag} and annealing on substrates without pre-heating

Films deposited on substrates without pre-heating (T_s = RT) show enhanced absorption in the low-energy spectral region and no evident signature of LSPR (top panel in Figure 6). Only the sample with d_{Ag} = 5 nm has a feature in the imaginary part of ε_{eff} at ≈ 1.7 eV, suggesting that the film may be partially formed by isolated particles. Drude contribution term is necessary to accurately model ε_{eff} in samples with d_{Ag} = 0 and 8 nm only,

indicating that these films percolate, as confirmed by SEM (top panel in Figure 7). Optical characterization of samples without Cu (not shown) confirms that the Ag seeding film with $d_{Ag} = 12$ nm is percolated. Therefore, a moderate amount of Ag ($d_{Ag} = 2$ and 5 nm) does not lead to percolation on substrates with no pre-heating. The large infrared absorption of these films that does not follow Drude dispersion law can be explained by clusters of very closely located or touching nanoparticles, as it has been observed in films near the percolation threshold [29, 30, 41]. Values of d_{eff} increase with d_{Ag} but are smaller than for pre-heated substrates, confirming that now films are more packed.

Optical properties of samples annealed at 450 °C (middle panel in Figure 6) show an absorption peak around 2 eV that can be assigned to LSPR of isolated particles. It indicates the formation of islands as a result of film dewetting upon annealing [11, 28]. However, modelling ε_{eff} in samples without Ag seeds still requires the Drude term, implying that the film is also percolated. Likewise in pre-heated substrates, a shoulder in LSPR high energy side is observed in samples with Ag. Although these films are not percolated, they show a broad absorption peak centered at energies below 1 eV. It should be noted that films with more Ag content ($d_{Ag} = 5$ and 8 nm) have larger d_{eff} than those deposited on pre-heated substrates and subjected to the same annealing treatment. Scanning electron micrographs of samples with $d_{Ag} = 8$ nm and annealed at 450 °C (middle panel in Figure 7) show a (two-dimensional) film structure composed of large ($\gtrapprox 100$ nm) irregular particles and of circular-like particles with size in the range of few to few tens of nm. These two families can explain the double-peak structure of ε_{eff},

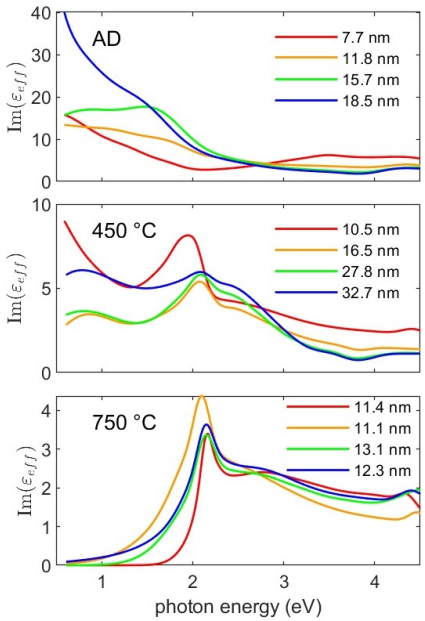

Figure 6: Imaginary part of the ε_{eff} for samples deposited on substrates without pre-heating (T_s = RT) with d_{Cu} = 5 nm and different d_{Ag} as a function of photon energy. Color lines indicate different Ag seeds: d_{Ag} = 0 (red), 2 (orange), 5 (green) and 8 nm (blue). Legend numbers indicate d_{eff} values for each sample. Top panel: as-deposited (AD) samples, middle panel: samples annealed at 450 °C, bottom panel: samples annealed at 750 °C.

since large, flat and irregular particles can be responsible of the low-energy peak [42]. Cross section and plain view STEM-EELS maps (Figure 8) reveal that irregular particles contain both Cu and Ag, with Cu preferentially in contact with the SiO_2 film surface. Height of these particles is ranging within several tens of nm, justifying the large values of d_{eff} in comparison with other samples. Such an irregular particle distribution results from the preferential dewetting of Ag, due to its lower surface energy than Cu.

Annealing at the highest temperature returns similar optical response and

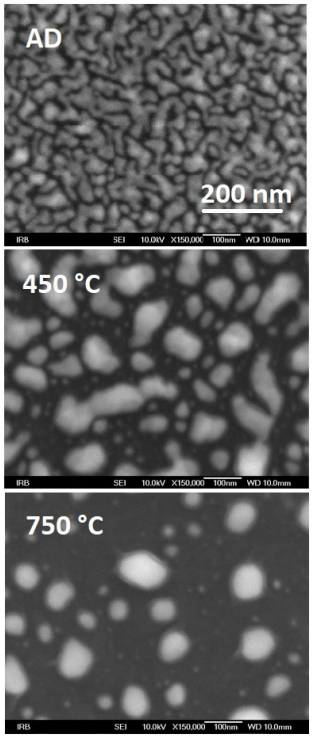

Figure 7: Scanning electron microscopy of sample with $d_{Cu} = 5$ nm and $d_{Ag} = 8$ nm deposited on substrates without pre-heating as deposited (top) annealed at 450 (middle) and at 750 °C (bottom). All micrographs are taken at the same magnification.

d_{eff} for all the samples (bottom panel in Figure 6). Compared to samples deposited on pre-heated substrates, even the one with $d_{Ag} = 8$ nm does not show evident Ag contribution to LSPR peak. As mentioned earlier, the Ag seeded film with $d_{Ag} = 8$ nm is percolated. Therefore the SiO_2 surface coverage is larger than in case of a film with the same Ag amount but formed by isolated nanoparticles. In this way, Cu deposition leaves a larger proportion of Ag exposed to the atmosphere than in pre-heated substrates, facilitating its evaporation upon annealing. EDS analysis of the sample annealed at 750

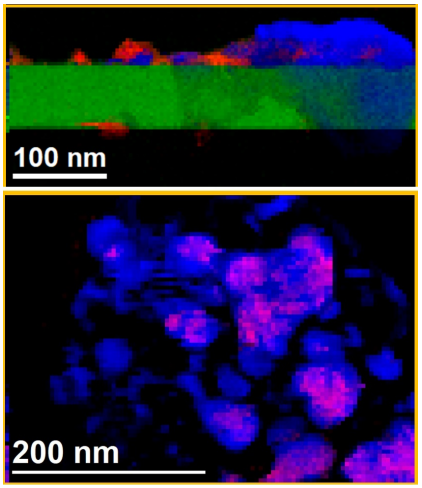

Figure 8: STEM-EELS map of samples with $d_{Ag} = 8$ nm and $d_{Cu} = 5$ nm deposited on substrates at T_s and annealed at 450 °C. Top panel illustrates cross section and lower panel a plain view of the sample surface. Composition maps show the distribution of Cu (red), Ag (blue) and O (green).

°C confirmed the absence of Ag.

The shape evolution upon annealing of as-deposited samples can be divided in two steps: In the first step, which occurs already at 450 °C the interconnected structure begins to break apart into isolated and irregular nanoislands due to Rayleigh-like instability [43]. In the second step, which occurs when annealing at 750 °C, all the silver evaporates and the remaining copper nanoislands take a more regular and round shape. A very similar morphological evolution of nanoislands following silver evaporation at high temperature in [44] was explained by minimization of surface energy by the remaining nanoislands attaining equilibrium shape.

3.4. Influence of d_{Cu}

In general terms, when a larger amount of Cu is deposited ($d_{Cu} = 10$ nm) results are qualitatively similar to those described so far. For deposition on pre-heated substrates, larger d_{eff} values and red-shifted LSPR are obtained in comparison to films with $d_{Cu} = 5$ nm (left column in Figure 9). In addition, the LSPR high energy shoulder displays a smaller weight due to the decreased Ag fraction in these samples. Moderate annealing (450 °C) results in LSPR blue shift and d_{eff} increase, as it happens in samples with smaller Cu amount. Differences in d_{eff} for films with $d_{Ag} \neq 0$ annealed at 450 °C and 750 °C are less remarkable than in samples deposited on pre-heated substrates. This observation indicates that Ag evaporates more easily with less Cu, for Ag is more exposed at the film surface and more weakly held by Cu because the two metals have smaller contact surface.

Optical properties of as-deposited films with $d_{Cu} = 10$ nm prepared without substrate pre-heating show Drude-like absorption, indicating that all films are percolated. Upon annealing at 450 °C, the Drude term contribution does not disappear from any of the samples. Although the films are percolated, they are less packed -as seen by the increase of d_{eff}- suggesting that the dewetting process is still at the hole propagation regime [45]. High temperature annealing yields well-defined LSPR peak in all samples. For Ag-containing films, values of d_{eff} are moderately lower or even larger than after annealing at 450 °C. In addition, the LSPR high energy shoulder is present even when $d_{Ag} = 2$ nm. These observations imply that the metal island films still contain a significant Ag fraction and, like in the case of deposition on pre-heated substrates, confirm that larger d_{Cu} aids to prevent Ag

evaporation.

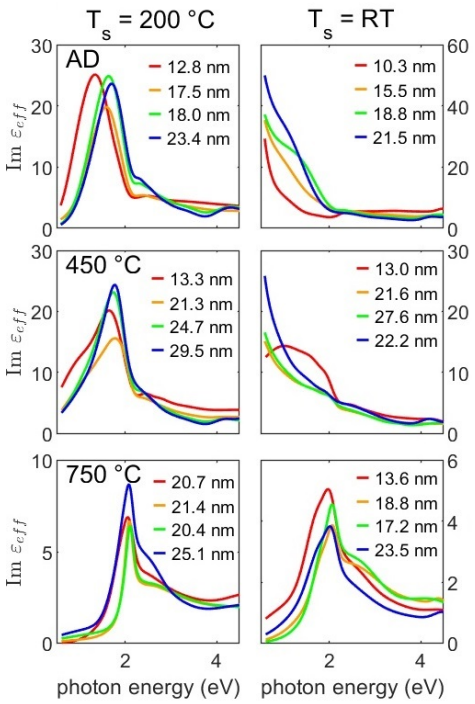

Figure 9: Imaginary part of ε_{eff} for samples deposited on pre-heated (left column, T_s = RT) and not pre-heated substrates (right column, T_s = 200 °C) with d_{Cu} = 5 nm and different d_{Ag} as a function of photon energy. Color lines indicate different Ag seeds: d_{Ag} = 0 (red), 2 (orange), 5 (green) and 8 nm (blue). Legend numbers indicate d_{eff} values for each sample. Top panel: as-deposited (AD) samples, middle panel: samples annealed at 450 °C, bottom panel: samples annealed at 750 °C.

3.5. Aging effects

Finally, we investigate the changes in optical properties of as-deposited samples with time inasmuch as Cu is prone to oxidize upon exposure to normal atmosphere [31]. Figure 10 shows transmittance spectra of samples with d_{Ag} = 0 and 8 nm deposited onto substrates with and without pre-heating.

Due to the progressive oxidization of Cu that quenches the LSPR, samples with no Ag show a transmittance increase with time. In addition, the film deposited on a pre-heated substrate shows LSPR red-shift versus time. This is explained by the gradual increase of the effective refractive index of the medium around the islands as it follows from the high refractive index of copper oxide [46, 47]. This variation cannot be confirmed for the sample deposited without pre-heating because LSPR peak falls out from the measured spectral range. It should be noted a slight decrease of transmittance with time for wavelengths below 400 nm that can be related to the Cu_2O interband transition at 3.5 eV [47].

Optical properties of films containing Ag present a significantly different time evolution. First, the sample deposited on a substrate without pre-heating shows weaker temporal variation than the other samples here discussed. This sample corresponds to the most packed film and has the smallest fraction of Cu in direct contact with the atmosphere, hence being less affected by Cu oxidization. The observed changes are a slight blue-shift and narrowing of the transmittance dip. These changes suggest that oxidized Cu regions reduce the number of possible electron paths along the film as it becomes, from an electro-optical point of view, a less percolated network. In this way, LSPR-like properties can more clearly emerge from the optical spectra. Lastly, the sample deposited on a pre-heated substrate is the only one whose transmittance decreases with time. As Cu is replaced by its oxide, LSPR becomes dominated by the Ag seed that has better plasmonic properties than Cu. Alongside, seeds get surrounded by a high refractive index medium (Cu_2O) which further strengthens but also red-shifts LSPR.

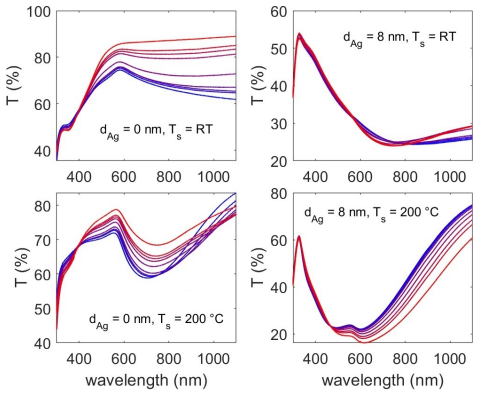

Figure 10: Transmittance spectra of samples with $d_{Cu} = 5$ nm and $d_{Ag} = 0$ (left column) or 8 nm (right column) and deposited on substrares without pre-heating (top) and pre-heated substrates (bottom) . Measurements were taken at different time intervals after deposition: 5 minutes, 30 minutes, 1 hour, 3 hours, 1 day, 1 week, 2 weeks, 3 weeks and 2 months. Line color continuously varies from the shortest (blue) to the longest time (red) after deposition.

4. Conclusions

It has been shown that optical properties of Cu-Ag metal island films deposited by electron beam evaporation can be broadly tailored by controlling fabrication conditions. The interplay between the amount of deposited materials, substrate deposition temperature and post-deposition annealing enables to modify film structure, islands morphology and composition. As a result, the optical properties can be varied from a metal-like behavior dominated by the Drude contribution at low energies to well-defined localized surface plasmon resonances with line-shape depending on the island composition and morphology.

It is observed that Ag seeds can quench film percolation, enhancing island formation. Thermal annealing at moderate temperatures results in island

growth and morphological changes that favour Janus-like structures. In case of percolated films, annealing induces dewetting that can result in large irregular particles in addition to smaller islands with LSPR in the visible range. Annealing at high temperature brings to partial Ag evaporation and film properties become primarily dominated by Cu. Time evolution of the optical response shows different trends depending on the film structure. Overall, the present study demonstrates that the optical properties of these samples can be broadly varied by adjusting a number of easily controllable fabrication parameters. A large tuning degree and a well-established fabrication technique therefore make Cu on Ag hybrid metal island films an attractive candidate for plasmonic applications.

Acknowledgements

The authors thank the financial support of the Croatian Science Foundation through the grant number IP-2019-04-5424. M. C. Spadaro and J. Arbiol acknowledge funding from Generalitat de Catalunya 2017 SGR 327. ICN2 is supported by the Severo Ochoa program from Spanish MINECO (Grant No. SEV-2017-0706) and is funded by the CERCA Programme / Generalitat de Catalunya. M.C.S. has received funding from the European Union's Horizon 2020 research and innovation programme under the Marie Skłodowska-Curie grant agreement No. 754510 (PROBIST) and the Severo Ochoa programme. Authors acknowledge F.J. Belarre for the TEM sample preparation.

References

[1] G. V. Naik, V. M. Shalaev, A. Boltasseva, Alternative plasmonic materials: beyond gold and silver, Advanced Materials 25 (24) (2013) 3264–3294.

[2] P. R. West, S. Ishii, G. V. Naik, N. K. Emani, V. M. Shalaev, A. Boltasseva, Searching for better plasmonic materials, Laser & Photonics Reviews 4 (6) (2010) 795–808.

[3] W. T. Hsieh, P. C. Wu, J. B. Khurgin, D. P. Tsai, N. Liu, G. Sun, Comparative analysis of metals and alternative infrared plasmonic materials, Acs photonics 5 (7) (2017) 2541–2548.

[4] J. B. Khurgin, Replacing noble metals with alternative materials in plasmonics and metamaterials: how good an idea?, Philosophical Transactions of the Royal Society A: Mathematical, Physical and Engineering Sciences 375 (2090) (2017) 20160068.

[5] M. G. Blaber, M. D. Arnold, M. J. Ford, A review of the optical properties of alloys and intermetallics for plasmonics, Journal of Physics: Condensed Matter 22 (14) (2010) 143201.

[6] M. B. Cortie, A. M. McDonagh, Synthesis and optical properties of hybrid and alloy plasmonic nanoparticles, Chemical reviews 111 (6) (2011) 3713–3735.

[7] S. A. Mezzasalma, V. Janicki, K. Salamon, J. Sancho-Parramon, Combination law for Drude–Sommerfeld's electron damping in multilayer thin

metal films, Physica Status Solidi (RRL)–Rapid Research Letters 12 (9) (2018) 1800149.

[8] N. Kaiser, Review of the fundamentals of thin-film growth, Applied optics 41 (16) (2002) 3053–3060.

[9] V. Gervilla, G. Almyras, F. Thunström, J. E. Greene, K. Sarakinos, Dynamics of 3D-island growth on weakly-interacting substrates, Applied Surface Science 488 (2019) 383–390.

[10] J. Sancho-Parramon, V. Janicki, M. Lončarić, H. Zorc, P. Dubček, S. Bernstorff, Optical and structural properties of Au-Ag islands films for plasmonic applications, Applied Physics A 103 (3) (2011) 745–748.

[11] Y. Oh, J. Lee, M. Lee, Fabrication of Ag-Au bimetallic nanoparticles by laser-induced dewetting of bilayer films, Applied Surface Science 434 (2018) 1293–1299.

[12] F. Hubenthal, N. Borg, F. Träger, Optical properties and ultrafast electron dynamics in gold–silver alloy and core–shell nanoparticles, Applied Physics B 93 (1) (2008) 39.

[13] H.-G. Boyen, A. Ethirajan, G. Kästle, F. Weigl, P. Ziemann, G. Schmid, M. Garnier, M. Büttner, P. Oelhafen, Alloy formation of supported gold nanoparticles at their transition from clusters to solids: Does size matter?, Physical review letters 94 (1) (2005) 016804.

[14] C. T. Langlois, T. Oikawa, P. Bayle-Guillemaud, C. Ricolleau, Energy-filtered electron microscopy for imaging core–shell nanostructures, Journal of Nanoparticle Research 10 (6) (2008) 997–1007.

[15] C. Wadell, A. Yasuhara, T. Sannomiya, Asymmetric light absorption and radiation of ag–cu hybrid nanoparticles, The Journal of Physical Chemistry C 121 (48) (2017) 27029–27035.

[16] S. Dubkov, A. Savitskiy, A. Y. Trifonov, G. Yeritsyan, Y. P. Shaman, E. Kitsyuk, A. Tarasov, O. Shtyka, R. Ciesielski, D. Gromov, SERS in red spectrum region through array of Ag–Cu composite nanoparticles formed by vacuum-thermal evaporation, Optical Materials: X 7 (2020) 100055.

[17] P. Nandhagopal, A. K. Pal, D. B. Mohan, Fabrication of silver and silver-copper bimetal thin films using co-sputtering for SERS applications, Optical Materials 97 (2019) 109381.

[18] M. Hirai, A. Kumar, Wavelength tuning of surface plasmon resonance by annealing silver-copper nanoparticles, Journal of applied physics 100 (1) (2006) 014309.

[19] A. Yasuhara, K. Kubo, S. Yanagimoto, T. Sannomiya, Thermodynamic tuning of Au–Ag–Cu nanoparticles with phase separation and ordered phase formation, The Journal of Physical Chemistry C 124 (28) (2020) 15481–15488.

[20] X. Zhang, S. Xu, S. Jiang, J. Wang, J. Wei, S. Xu, S. Gao, H. Liu, H. Qiu, Z. Li, et al., Growth graphene on silver–copper nanoparticles by chemical vapor deposition for high-performance surface-enhanced raman scattering, Applied Surface Science 353 (2015) 63–70.

[21] A. K. Pal, D. B. Mohan, Sers enhancement, sensitivity and homogeneity studies on bi-metallic Ag-Cu films through tuning of broad band SPR towards red region, Journal of Alloys and Compounds 698 (2017) 460–468.

[22] C. Langlois, Z. Li, J. Yuan, D. Alloyeau, J. Nelayah, D. Bochicchio, R. Ferrando, C. Ricolleau, Transition from core–shell to Janus chemical configuration for bimetallic nanoparticles, Nanoscale 4 (11) (2012) 3381–3388.

[23] S. Li, W. Qi, H. Peng, J. Wu, A comparative study on melting of core–shell and Janus Cu–Ag bimetallic nanoparticles, Computational Materials Science 99 (2015) 125–132.

[24] W. T. Osowiecki, X. Ye, P. Satish, K. C. Bustillo, E. L. Clark, A. P. Alivisatos, Tailoring morphology of Cu–Ag nanocrescents and core–shell nanocrystals guided by a thermodynamic model, Journal of the American Chemical Society 140 (27) (2018) 8569–8577.

[25] H. Peng, W. Qi, S. Li, W. Ji, Modeling the phase stability of Janus, core–shell, and alloyed Ag–Cu and Ag–Au nanoparticles, The Journal of Physical Chemistry C 119 (4) (2015) 2186–2195.

[26] L. Vitos, A. Ruban, H. L. Skriver, J. Kollar, The surface energy of metals, Surface science 411 (1-2) (1998) 186–202.

[27] A. Jamnig, N. Pliatsikas, G. Abadias, K. Sarakinos, On the effect of copper as wetting agent during growth of thin silver films on silicon dioxide substrates, Applied Surface Science 538 (2020) 148056.

[28] H. Oh, A. Pyatenko, M. Lee, A hybrid dewetting approach to generate highly sensitive plasmonic silver nanoparticles with a narrow size distribution, Applied Surface Science 542 (2021) 148613.

[29] M. Hövel, B. Gompf, M. Dressel, Dielectric properties of ultrathin metal films around the percolation threshold, Physical Review B 81 (3) (2010) 035402.

[30] J. Sancho-Parramon, V. Janicki, H. Zorc, Tuning the effective dielectric function of thin film metal-dielectric composites by controlling the deposition temperature, Journal of Nanophotonics 5 (1) (2011) 051805.

[31] J. Sancho-Parramon, B. Okorn, K. Salamon, V. Janicki, Plasmonic resonances in copper island films, Applied Surface Science 463 (2019) 847–853.

[32] U. Hohenester, A. Trügler, MNPBEM–a Matlab toolbox for the simulation of plasmonic nanoparticles, Computer Physics Communications 183 (2) (2012) 370–381.

[33] P. B. Johnson, R.-W. Christy, Optical constants of the noble metals, Physical review B 6 (12) (1972) 4370.

[34] I. Fabijanić, V. Janicki, J. Ferré-Borrull, M. Bubaš, V. Blažek Bregović, L. F. Marsal, J. Sancho-Parramon, Plasmonic nanoparticles and island films for solar energy harvesting: A comparative study of Cu, Al, Ag and Au performance, Coatings 9 (6) (2019) 382.

[35] H. Ehrenreich, H. Philipp, Optical properties of ag and cu, Physical Review 128 (4) (1962) 1622.

[36] M. M. Schneider, J. M. Howe, Observation of interface dynamics and cu island formation at a crystalline si/liquid al-alloy interface, Acta Materialia 133 (2017) 224–229. doi:10.1016/j.actamat.2017.05.023.

[37] O. Stenzel, et al., The physics of thin film optical spectra, Springer, 2015.

[38] J. Margrave, The Characterization of High-temperature Vapors, Wiley, 1967.

[39] D. Alloyeau, G. Prévot, Y. Le Bouar, T. Oikawa, C. Langlois, A. Loiseau, C. Ricolleau, Ostwald ripening in nanoalloys: when thermodynamics drives a size-dependent particle composition, Physical review letters 105 (25) (2010) 255901.

[40] F. Bocquet, C. Maurel, J.-M. Roussel, M. Abel, M. Koudia, L. Porte, Segregation-mediated capping of Volmer-Weber Cu islands grown onto Ag (111), Physical Review B 71 (7) (2005) 075405.

[41] A. J. de Vries, E. S. Kooij, H. Wormeester, A. A. Mewe, B. Poelsema, Ellipsometric study of percolation in electroless deposited silver films, Journal of applied physics 101 (5) (2007) 053703.

[42] M. Bosman, E. Ye, S. F. Tan, C. A. Nijhuis, J. K. Yang, R. Marty, A. Mlayah, A. Arbouet, C. Girard, M.-Y. Han, Surface plasmon damping quantified with an electron nanoprobe, Scientific reports 3 (1) (2013) 1–7.

[43] J. Ye, C. V. Thompson, Templated solid-state dewetting to controllably

produce complex patterns, Advanced Materials 23 (2011) 1567–1571. doi:10.1002/adma.201004095.

[44] M. Sui, S. Kunwar, P. Pandey, J. Lee, Strongly confined localized surface plasmon resonance (LSPR) bands of Pt, AgPt, AgAuPt nanoparticles, Scientific Reports 9 (16582) (2019). doi:10.1038/s41598-019-53292-1.

[45] P. Jacquet, R. Podor, J. Ravaux, J. Teisseire, I. Gozhyk, J. Jupille, R. Lazzari, Grain growth: The key to understand solid-state dewetting of silver thin films, Scripta Materialia 115 (2016) 128–132.

[46] T. Ito, H. Yamaguchi, T. Masumi, S. Adachi, Optical properties of CuO studied by spectroscopic ellipsometry, Journal of the Physical Society of Japan 67 (9) (1998) 3304–3309.

[47] T. Ito, T. Kawashima, H. Yamaguchi, T. Masumi, S. Adachi, Optical properties of Cu_2O studied by spectroscopic ellipsometry, Journal of the Physical Society of Japan 67 (6) (1998) 2125–2131.